# ROUGHNESS DEVELOPMENT DURING DYNAMIC FRACTURE IN BRITTLE POLYMER

K. TAKAHASHI and M. KIDO*
*Research Institute for Applied Mechanics, Kyushu University*
*816 Kasuga, Japan*
**Presently, Yokohama Research Center, Mitsubishi Chemical Co.*
*1000 Kamoshida, Aoba-ku, 227 Yokohama, Japan*

## ABSTRACT

The development of roughness for dynamic fracture in epoxy specimens (Araldite B) was studied in relation to important fracture parameters of crack velocity $\dot{a}$, acceleration $\ddot{a}$ and stress intensity factors $K_{Id}$ during crack propagation. Dual-focus high speed photography was employed to evaluate values of $K_{Id}$ by the caustic ($K_{Id}$(C)) and photoelastic ($K_{Id}$(P)) methods simultaneously. A specially designed jig applied successive tensile loadings to specimens which resulted in cyclic change of $\dot{a}$ and $\ddot{a}$. The focus was primarily on the first half cycle of $\dot{a}$ in a comparison of changes of roughness RMS and other parameters. A typical result showed that the position of the first maximum value of $\dot{a}$ came almost on the first loading axis, while that of $K_{Id}$ (P), RMS and $K_{Id}$ (C) appeared on the fracture surface 7mm, 15mm, and 25mm behind the axis, respectively. The maximum peak of RMS roughly coincided with the peak of deceleration.

## KEY WORDS

Roughness development, dynamic fracture, dynamic stress intensity factor, caustic method, photoelastic method, crack velocity, crack acceleration.

## INTRODUCTION

Roughness developed during a course of rapid crack propagation in brittle, or semi-brittle, polymers has been studied from various aspects (Cotterell, 1968; Ravi-Candar and Knauss, 1984; Arakawa and Takahashi, 1991a; Hull, 1995, 1996), with the dependence of the roughness RMS on the stress intensity factor during crack propagation $K_{Id}$, crack velocity $\dot{a}$ and other fracture parameters one focus. Using the method of caustics Arakawa and Takahashi (1991a) indicated for three kinds of glassy polymers, i.e., PMMA, epoxy (Araldite D) and cross-linked polyester (Homalite 100) that neither the crack velocity $\dot{a}$ nor $K_{Id}$ was uniquely related with RMS, but each of those materials had a different cause of roughness origination in the crack velocity ranges studied. Parabolic markings were primarily responsible in PMMA, whereas pit marks in Araldite D and difference in level as well as pit marks in Homalite 100. Based on experimental results of the roughness measurement and also on the crack branching (Arakawa and Takahashi, 1991b), they proposed a parameter $R^*\dot{a}$. There was a linear increase of RMS with $R^*\dot{a}$, where $R^*$ is a dynamic component of the crack extension resistance.

Considering roughness studies from a technical viewpoint we may have still factors requiring further investigation. For example, neither a mechanical roughness meter nor a non-contact optical roughness meter is adequate to examine fracture surfaces which have a roughness varying from fine to course ( Hull, 1996). Few studies have been done (Nigam and Shukla, 1988; Yang *et al.*, 1988) on the coincidence problem of $K_{Id}$ values obtained by the caustic and the photoelastic methods under dynamic conditions and we do not have enough quantitative information to correlate the two kinds of values obtained from a single fracture event. Values of roughness have rarely been correlated with those of acceleration.

In the present study, the authors sought to relate the roughness of epoxy with as many other mechanical parameters as possible determined simultaneously for one specimen to gain a better view of this dynamic fracture problem. A dual-focus Cranz-Schardin camera was developed for this purpose.

## EXPERIMENTAL

### *Photography system*

A Cranz-Schardin type dual focus camera (Takahashi and Mada, 1992) was utilized to determine crack length $a$ and the other parameters $\dot{a}(a)$, $\ddot{a}(a)$ and $K_{Id}(a)$. The camera had 30 lenses and the same number of spark light sources. Figure 1 shows the optical setup for dual focus high speed photography. Light beams incident to the camera lenses were split into two directions by a beam splitter in the camera box. Each of the sheet films ($F_1$ and $F_2$) was focused on a different image plane ($I_1$ and $I_2$). The dual focus system shown in Fig. 1 is for simultaneous determination of $K_{Id}(a)$ by both photoelastic and caustic methods. The optical path from $I_1$ to $F_1$ was for the photoelastic photography and that from $I_2$ to $F_2$ for the caustic photography. A similar system was earlier adopted by way of trial by the authors' group (Yang *et al.*, 1988) using a prototype camera (Takahashi and Arakawa, 1987) on the basis of a successful result of simple dual focus high speed photography (Arakawa and Takahashi 1987). The presently modified camera was equipped with spark light sources greatly intensified for the simultaneous caustic and photoelastic photography.

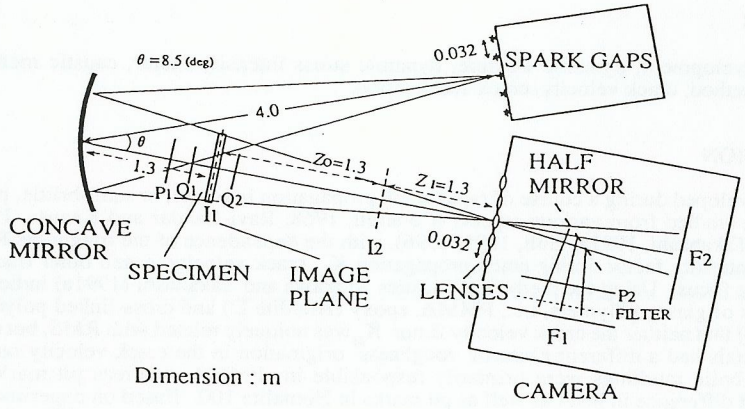


Fig. 1 Optical setup for simultaneous caustic and photoelastic high speed photography.



### *Parallax error correction of the camera*

To improve the accuracy in quantitative measurements with the camera, the effect of parallax with the 30 lenses was experimentally evaluated in the determination of caustic diameter $D$ (Kido and Takahashi, 1994). Figure 2(a) shows the sequence of photographs with the 30 lenses. Caustic images of an SEN-PMMA specimen under static tension were photographed by film $F_2$ in Fig. 1. A caustic image from frame no. 11 was chosen from among 30 frames as a standard in the present calibration procedure because of its distinctness in the photographed pattern. Caustic diameters were measured on the film using an optical magnifier and were correlated with that of frame No. 11. Thus, correction factors were obtained for other lenses as shown in Fig. 2(b).

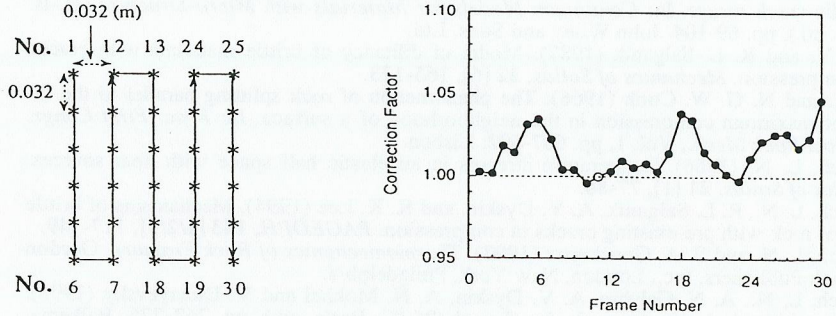


Fig. 2 Sequence of photography with 30 lenses (a), and correction factors for the measurement of caustic diameters (b).

### *Determination of roughness and other mechanical parameters*

A non-contact optical profilometer (Zygo New View 100) was used for the roughness evaluation up to the maximum value of 40 $\mu$ m. The measurement was performed as shown by Fig.3. The roughness at the $i-$th point (see Fig. 3) was obtained from a characteristic area $1 \times 1 \text{mm}^2$ where the profilometer measured an averaged value RMS

$$\text{RMS} = \sqrt{\frac{1}{l}\int_0^l f(x)^2 \cdot dx} \quad (1)$$

where $l = 1\,mm$ and $f(x)$ is the roughness profile curve.

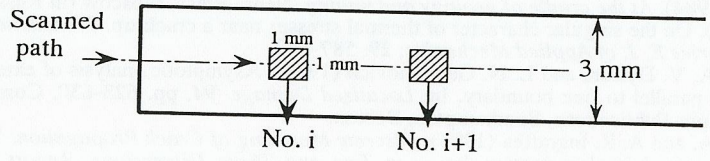


Fig. 3 Non-contact profilometry of fracture surface.

k length $a$ was obtained from the photoelastic series as a function of time and the curve of was represented by a 9th order polynomial based on the least square concept, as reported er by Takahashi and Arakawa (1987)

$$= \sum_{i=0}^{9} a_i t^i \qquad (2).$$

crack velocity $\dot{a}$ and acceleration $\ddot{a}$ were determined by the time derivative of $a(t)$ and $\dot{a}(t)$, ectively.

ues of the dynamic stress intensity factor during crack propagation were obtained simultaısly as mentioned above using the following formulae

$$= const \cdot F(\dot{a}) D^{3/2} / Z_o cd \qquad (3)$$

$$(P) = (Nf_d/d)\sqrt{2\pi r_m} H(\theta_m, \dot{a}) \qquad (4)$$

re $F(\dot{a})$ is the dynamic correction factor (Beinert and Kalthoff, 1981), $Z_o$ is the distance veen specimen and the image plane $I_2$ ( see Fig. 1), $c$ is stress optical constant, $d$ is thickness ıe specimen, $N$ is isochromatic fringe number, $f_d$ is dynamic photoelastic coefficient, $r_m$ is maximum distance of the isochromatic fringe pattern from the crack tip, $H$ is dynamic corion factor (Irwin, 1958) and $\theta_m$ is angle of the fringe pattern corresponding to $r_m$.

### cimens and loading jig

es of epoxy (Araldite B) with geometries of 120×150×3 (mm) (see Fig. 4(a)) were used, a specific loading jig (Arakawa *et al.*, 1996) shown in Fig 4 (b) was machined. The jig is gned to apply a tensile loads twice for a running crack, which should cause successive accelion-deceleration cycles. The roughness development procedure was thus studied under situns more complex than these employed previously to learn the effects of various factors. The hand side of the specimen in Fig. 4 (a) can be considered as one SEC-CT specimen kahashi and Arakawa, 1987) and the right-hand side another SEC-CT specimen; Actually, n of the SEC-CT systems is accompanied by biaxiality in the loading, although the effect of biaxiality is neglected in the following discussion.

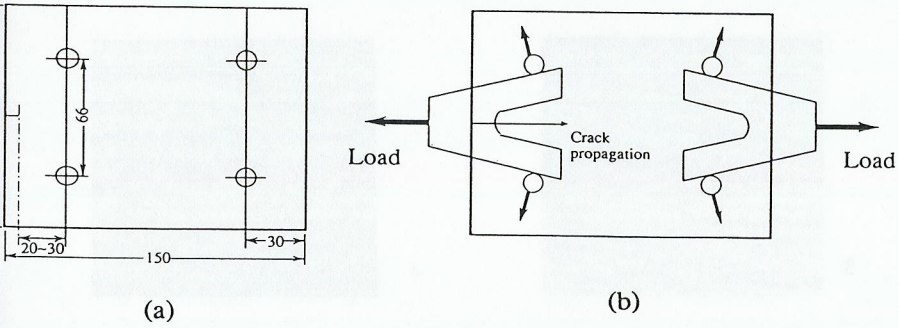


Fig. 4 Specimen geometries (a) and loading jig (b).



## RESULTS AND DISCUSSION

### Crack velocity change

Figures 5 (a) and (b) show the crack velocity change for an epoxy specimen as a function of the crack length and time, respectively; a distinct velocity oscillation can be seen. Here, in addition to the two velocity peaks corresponding to the successive tensile loads, there is another velocity peak. This additional peak was probably generated by vertical oscillation of the specimen which would have taken place when the first acceleration-deceleration cycle ended. It is noted that PMMA with higher molecular weight ($\sim 10^6$) and epoxy (Araldite D) specimens with a thickness of 5mm show this third peak only slightly (see Fig. 5 (c)). So it appears that thin and brittle materials like the present specimens tend to exhibit this peak distinctly. The position of the first peak of $\dot{a}$ ($a$) almost coincided with that of the first tensile loading axis, whereas in PMMA it came afterward. The second peak of $\dot{a}$ in Fig. 5(a) was located behind the second tensile load axis. This change in situation might result from a superposition of the oscillation and other dynamic effects. Figure 5 (a) shows the maximum values of acceleration obtained in the rising and falling parts of the first and second peaks, respectively. Values of $\ddot{a}$ are on the order of $10^5 \sim 10^6$ m/s$^2$.

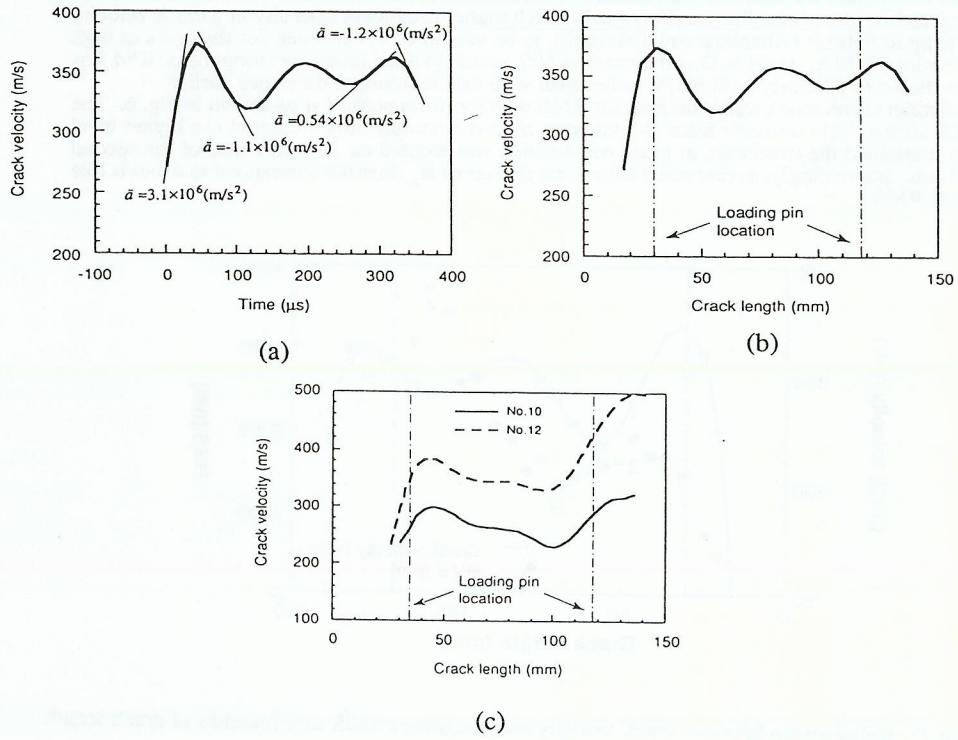


Fig. 5 Typical crack velocity change in a specimen as a function of time (a) and crack length (b). Typical examples of specimens of PMMA (5mm thick) (c).

*Roughness development*

Figure 8 shows typical fracture surface topography for one specimen. (Here, the numbers 1-4 correspond to those in Fig. 6. ) In a stage of low crack velocity (no. 1; 265 m/s) pit marks are mostly associated with the roughness. With an increase of $\dot{a}$, longitudinal broad line markings which contained fine lines were significant together with undulatory facets (no. 2; 320m/s). The length of the broad line tended to decrease when $\dot{a}$ decreased (no. 3; 300m/s) and then again increased both in length and width when the crack approached the second tensile axis (no.4; 390 m/s). Figure 6 shows the dependence of RMS on $\dot{a}$. The RMS in the first SEC-CT part showed a delay in its change with crack length as compared with that of crack velocity. This tendency is qualitatively in accord with that previously reported by Arakawa and Takahashi for single SEC-CT specimens of PMMA, Araldite D and Homalite 100 (1991a), although the extent of roughness was much less in these studies and the main causes for the roughness origination were different. Crack bifurcation, or successive branching into multiple cracks, can be considered an extreme case of roughness development. In this context, it is not unusual for the bifurcation to take place even during crack deceleration, as shown by Arakawa and Takahashi for Araldite D and Homalite 911 (CR-39) (1991b).

Figure 7 shows that the peak of RMS almost corresponds with that of deceleration. A similar result is obtained for SEC-CT specimens of PMMA with lower molecular weight which exhibit characteristic transverse line markings with much higher roughness intensity in a crack velocity range up to 550m/s (Aboelezz and Takahashi, to be submitted). However, for the cases of high molecular PMMA, Araldite D and Homalite 100, which yielded much less roughness, $R^*\dot{a}$ has been shown to fit nicely with RMS, rather than with deceleration, as described earlier.
No distinct correlations were obtained for RMS with the third peak of $\dot{a}$ as shown in Fig. 6. The RMS, after a slight decrease from its first peak, almost monotonically increased to a higher level until it attained the maximum at place no. 4 which was located ca. 10 mm ahead of the second load axis. Interestingly, as discussed below, the change of $K_{Id}$ does not correspond to $\dot{a}$ but is like that of RMS.

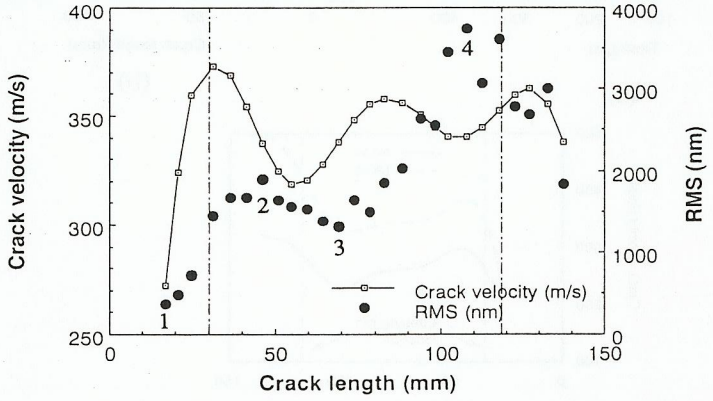


Fig. 6 Relationship between crack velocity and roughness RMS as a function of crack length (numbers 1-4 correspond to those in Fig. 8).



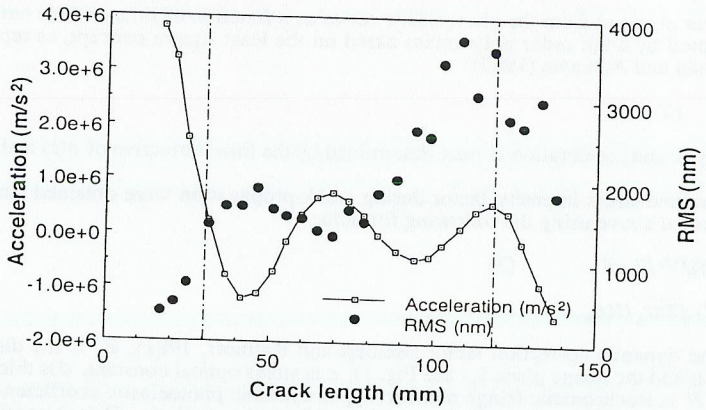


Fig. 7 Relationship between crack acceleration and RMS.

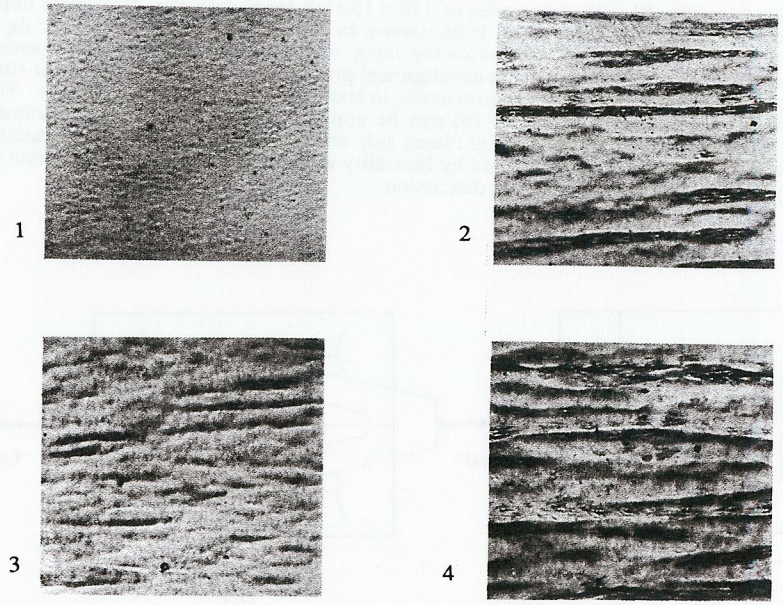


Fig. 8 Fracture surface appearance at places 1-4 indicated in Fig. 6 by the corresponding numbers. Actual sizes of each photograph are 1mm by 1mm.

*ynamic stress intensity factor*

gure 9 is an example of the simultaneously obtained high speed pictures of caustics and isochmatic fringes for the specimen described above. The experimental condition of photography is own in Fig. 1. Values of the initial curve radius $r_o$ of the caustics in this case were in a range $9 < r_o/h < 1.3$ where $h$ is the specimen thickness, while the radius $r$ of the isochromatic fringe as in a range $1.5 < r/h < 3.0$. Therefore, the evaluation of $K_{Id}$ was made based on the stress stribution at different places which were a few millimeters apart. The quality of the isochroatic fringe pictures is not satisfactory mainly because of insufficient light intensity; this was e to the requirement to take sharp caustic images using light sources as small as possible in ze.

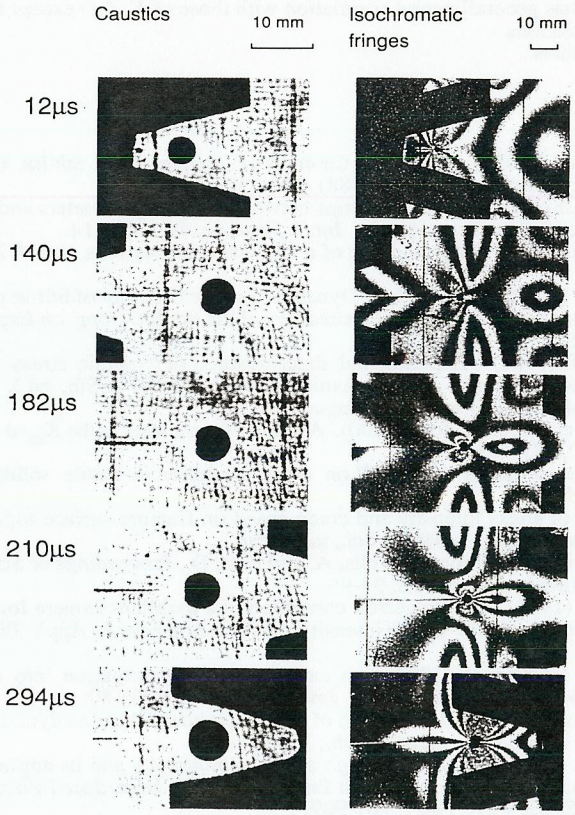


Fig. 9 Selected pictures of simultaneously taken caustics and photoelastic fringes.



Figures 10 and 11 show experimental results of $K_{Id}$(C) and $K_{Id}$(P) in comparison with the change of RMS. Qualitatively, there seems to be a much better correlation between RMS and $K_{Id}$(C), or $K_{Id}$(P), than the case of RMS versus $\dot{a}$, where $\dot{a}$ exhibited the additional peak between the loading axes as described above. Quantitatively, however, there are discrepancies. The first and second peak positions of $K_{Id}$(C) and of $K_{Id}$(P) differ from those of RMS. Tables 1 and 2 summarize the results of the peak positions for $\dot{a}$, $\ddot{a}$, RMS and $K_{Id}$ near the first and second loading axis, respectively.

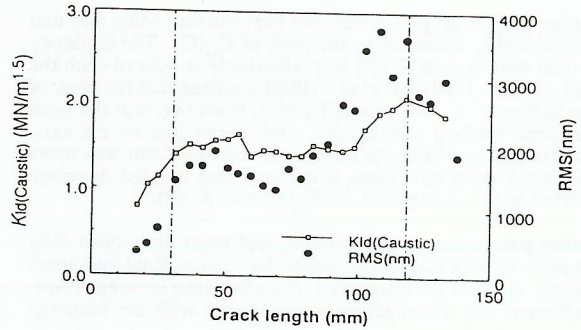


Fig. 10 Relationship between $K_{Id}$ (caustic) and RMS.

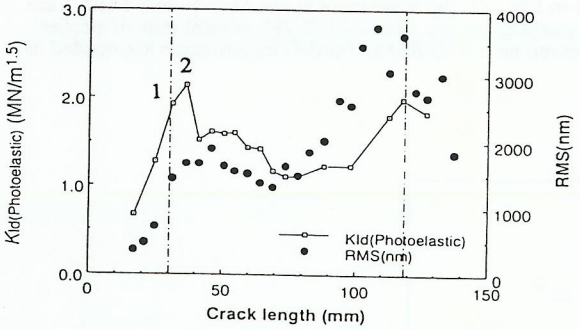


Fig. 11 Relationship between $K_{Id}$ (photoelastic) and RMS (numbers 1 and 2 correspond to those in Fig. 12).

| | (1st load axis) | $\dot{a}$ | $\ddot{a}$ | RMS | $K_{ID}$(C) | $K_{ID}$(P) |
|---|---|---|---|---|---|---|
| $a$ (mm) | (30) | 32 | 42 | 45 | 55 | 37 |

Table 1 Crack lengths representing peak positions of fracture parameters associated with first loading

| | (2nd load axis) | $\dot{a}$ | $\bar{a}$ | RMS | $K_{ID}$(C) | $K_{ID}$(P) |
|---|---|---|---|---|---|---|
| $a$ (mm) | (118) | 126 | 118 | 108 | 118 | 118 |

Table 2 Crack lengths representing peak positions of fracture parameters associated with second loading

In Table 1 the peak of $\dot{a}$ precedes all other parameter peaks near the first loading axes, and that the peak of $K_{Id}$(P) comes earlier than that of RMS, followed by the peak of $K_{Id}$(C). The tendency for the peak of $K_{Id}$(C) to come slightly later than that of $K_{Id}$(P) is qualitatively in accord with the result for Araldite D given by Yang, *et al.* (1988). Dally, ad *et al.* (1990) reported that the peak of $K_{Id}$(P) for Homalite 100 was quite close to that of $\dot{a}$. We see in Table 2, however, that the peak positions of $K_{Id}$(C) and $K_{Id}$(P) at the second loading axis agreed, and came just on the axis. Values of RMS were more scattered in this region where the roughness development was more intensive with no noticeable increase in crack velocity. Thus, it is concluded that the development of roughness cannot be simply related to the changes of $\dot{a}$, $K_{Id}$(C) and $K_{Id}$(P).

The effect of the third peak of $\dot{a}$ on other parameters is not evident, and must have been only slight, if any at all. As discussed, this peak is believed to be caused by longitudinal specimen oscillation, not by initial stress distribution. It is not accompanied by an increase in stress intensity factor. This situation may have effected this discrepancy as compared with the loadings along the first and second axes.

Figure 12 shows the relationship between $K_{Id}$(C) and $K_{Id}$(P). Except for the two points 1 and 2, which correspond to the same numbers in Fig. 11, the agreement is not bad. Points 1 and 2 are located in Fig. 11 at higher positions pushing up the values of $K_{Id}$(P) several tens of percent. However, no discernible change is observed here with RMS. Further experiments are needed to verify these results.

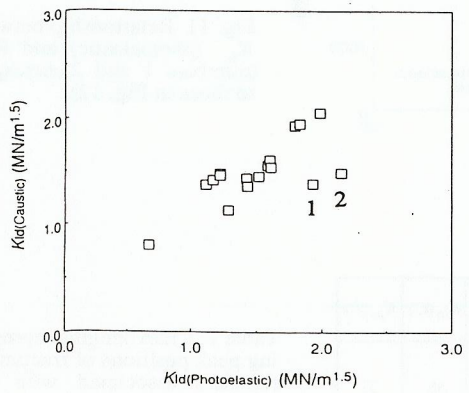


Fig. 12 Correlation between $K_{Id}$ (caustic) and $K_{Id}$ (photoelastic).



## CONCLUSIONS

The development of roughness was studied during fast fracture in thin Araldite B plates under successive tensile loads in relation to several important fracture parameters which were simultaneously evaluated by dual focus high speed photography, and the following conclusions obtained.

1. The peak of $\dot{a}(a)$-curve precedes peaks of RMS $(a)$-, $K_{Id}$(photoelastic) $(a)$-, $K_{Id}$ (caustic)$(a)$- and RMS$(a)$-curve at the first tensile load axis, where the peak of RMS$(a)$-curve corresponds to that of deceleration and the peak of $K_{Id}$(photoelastic)$(a)$ comes earlier than those of RMS and *KId (caustic)*$(a)$.
2. The third crack velocity peak appears between two peaks at the tensile axes. This peak does not correspond to any peaks of RMS $(a)$ or $K_{Id}(a)$.
3. The correlation between $K_{Id}$(photoelastic) $(a)$ and $K_{Id}$(caustic)$(a)$ is fairly good except for their peak positions at the first load axis.
4. The change of RMS $(a)$ has generally good correlation with those of $K_{Id}(a)$ except for slight discrepancies in the peak positions.

Captions of Figures and Tables

## REFERENCES


Arakawa, K. and K. Takahashi (1988). A criterion for crack branching. *Proc. 6th Int. Congress on Experimental Mechanics* (SEM, 1988), 746-750.

Arakawa, K. and K. Takahashi (1991a). Relationships between fracture parameters and fracture surface roughness of brittle polymers. *Int. J. Fracture*, 48, 103-114.

Arakawa, K. and K. Takahashi (1991b). Branching of a fast crack in polymers. *Int. J. Fracture*, 48, 245-254.

Arakawa, K., D. Nagoh and K. Takahashi (1996). Dynamic fracture behavior of brittle polymers under biaxial loading. In: *Abstract Proceedings of the 8th Int. Cong. on Exp. Mech.*, pp. 349-350. SEM.

Beinert, J. and J. F. Kalthoff (1981). Experimental determination of dynamic stress intensity factors by shadow patterns. In: *Mechanics of fracture* (G. C. Sih, ed.), Vol. 7, pp. 281-330. Martinus Nijhoff, The Hague.

Dally J. W., R. K. Agarwal and R. J. Sanford (1990). A study of hysteresis in the $K_{ID}$- $\dot{a}$ relation. *Exp. Mech.*, 30, 177-183.

Hull, D. (1995). The effect of mixed mode I/III on crack evolution in brittle solids. *Int. J. Fracture*, 70, 59-79.

Hull, D. (1996). Influence of stress intensity and crack speed on fracture surface topography: Mirror to mist transition. *J. Mater. Sci.*, to appear.

Irwin, G. R. (1958). Discussion to a paper of Wells, A. and Post, D., *Proceedings of Society for Experimental Stress Analysis*, 16, 93-96.

Kido, M. and K. Takahashi (1994). Parallax error correction of a multilens camera for precise determination of dynamic stress intensity factor. *Japanese J. Appl. Phys.*, 33, L200-L203.

Ravi-Chandar, K. and W. G. Knauss (1984). An experimental investigation into dynamic fracture: II. Microstructural aspects. *Int. J. Fracture*, 26, 65-80.

Takahashi, K. and K. Arakawa (1987). Dependence of crack acceleration on the dynamic stress intensity factor in polymers. *Exp. Mech.*, 27, 195-200.

Takahashi, K. and T. Mada (1992). Dual focus high speed photography and its application to fracture and impact studies. *Proc. 20th Int. Congress on High-Speed Photography and Photonics SPIE*, Vol. 1801, 901-909.

Yang P.-T. , Y. Sakurada, T. Mada and K. Takahashi (1988). An attempt to simultaneously obtain the dynamic stress intensity factor by both photoelastic and caustic methods. *Bulletin of Research Institute for Applied Mechanics*, Kyushu University, No. 68, 543-550 (in Japanese).